

Cite this: *Polym. Chem.*, 2022, **13**,  
4650

## *meta*-Terphenyls as versatile fluorescent molecular sensors for monitoring the progress of hybrid polymerization processes

Wiktorja Tomal,<sup>a</sup> Patryk Szymaszek,<sup>a</sup> Magdalena Bilut,<sup>a</sup> Roman Popielarz,<sup>a</sup> Tomasz Świergosz<sup>†b</sup> and Joanna Ortyl<sup>†a</sup>

Herein, the performance of a series of 2-amino-4,6-diphenylbenzene-1,3-dicarbonitrile derivatives in the role of fluorescent molecular sensors for monitoring progress of various photopolymerization processes by the Fluorescence Probe Technique (FPT) has been evaluated. It was found that all of the derivatives studied, except for the one containing a nitro substituent in its structure, showed high enough sensitivity and stability to be applied as versatile sensors for both cationic and free-radical polymerization processes. Next, the applicability of the sensors was applied for study of hybrid polymerization processes (*i.e.*, both cationic and free radical polymerization reactions occurring simultaneously). The hybrid photopolymerization of pure glycidyl methacrylate (GlyMA) and the mixtures of GlyMA with 3,4-epoxycyclohexylmethyl 3,4-epoxycyclohexanecarboxylate (CADE), or CADE with trimethylolpropane triacrylate (TMPTA) was studied. It was found that during the hybrid photopolymerization of CADE/TMPTA mixtures, each monomer polymerized independently to form an interpenetrated polymer network (IPN). On the other hand, hybrid photopolymerization of GlyMA/CADE mixtures leads to a copolymer, where final functional group conversions are higher than those achievable by the corresponding photopolymerizations of pure GlyMA and CADE monomers. The use of *m*-terphenyl sensors allows for real-time monitoring of various hybrid polymerization processes and provides key information on the processes, which was not previously possible.

Received 25th April 2022,  
Accepted 21st June 2022

DOI: 10.1039/d2py00525e

rsc.li/polymers

## Introduction

Polymers have conquered not only the chemical market but also other sectors, such as biomedicine, allowing development of engineering materials for fabrication of artificial tissues,<sup>1,2</sup> protective coatings,<sup>3,4</sup> or materials for targeted drug delivery applications.<sup>5,6</sup> Various methods are used for polymer production. One of the most modern methods of polymer synthesis is photopolymerization.<sup>7–10</sup> The light-induced polymerization processes are highly-efficient, fast, solvent-free and economical.<sup>11–14</sup> Due to numerous advantages, photopolymerization is used in polymer coating industry,<sup>15</sup> and for solvent-free paints,<sup>16</sup> varnishes<sup>17</sup> and adhesives,<sup>18</sup> as well as in graphics industry.<sup>19,20</sup> Moreover, the photopolymerization processes have been used in 3D printing technology and microelectronics for encapsulation of integrated circuits.<sup>21–30</sup>

For a photopolymerization process to be efficient and the polymeric product having desired properties, it is necessary to control the photopolymerization course, preferably *on-line* (*i.e.*, directly during the reaction) or the process parameters need to be optimized. For this purpose, various techniques for monitoring the progress of the photopolymerization processes, such as Real Time Fourier-Transform Infrared Spectroscopy (RT-FTIR), Photo-Differential Scanning Calorimetry (Photo-DSC) and the Fluorescence Probe Technique (FPT) have been developed. In particular, the FPT has gained a lot of attention, because of its simplicity and versatility in both on-line and off-line uses.<sup>31–34</sup> In polymer chemistry, the FPT is employed to monitor the progress of polymerization and photopolymerization processes, as well as to control the quality of raw materials used for fabrication of polymers, including the parameters of the final products.<sup>35,36</sup> Moreover, this method can be employed to evaluate the kinetics of polymerization processes and to assess quantitatively the efficiency of various photoinitiators in order to optimize the photopolymerization process.<sup>37</sup> Comparing these methods, photo-DSC and photo-FTIR provide information about the direct changes that occur in the monomer/monomer mixture during photopolymerization processes, while the FPT gives direct information about the sensor behavior in a given process caused by

<sup>a</sup>Department of Biotechnology and Physical Chemistry, Faculty of Chemical Engineering and Technology, Cracow University of Technology, Warszawska 24, 31 155 Kraków, Poland. E-mail: jortyl@pk.edu.pl, rpopiel@pk.edu.pl

<sup>b</sup>Department of Chemical Technology and Environmental Analysis, Faculty of Chemical Engineering and Technology, Cracow University of Technology, Warszawska 24, 31 155 Kraków, Poland

†This paper is dedicated to the memory of Tomasz Świergosz who passed away on June 30, 2022, at the age of 36.



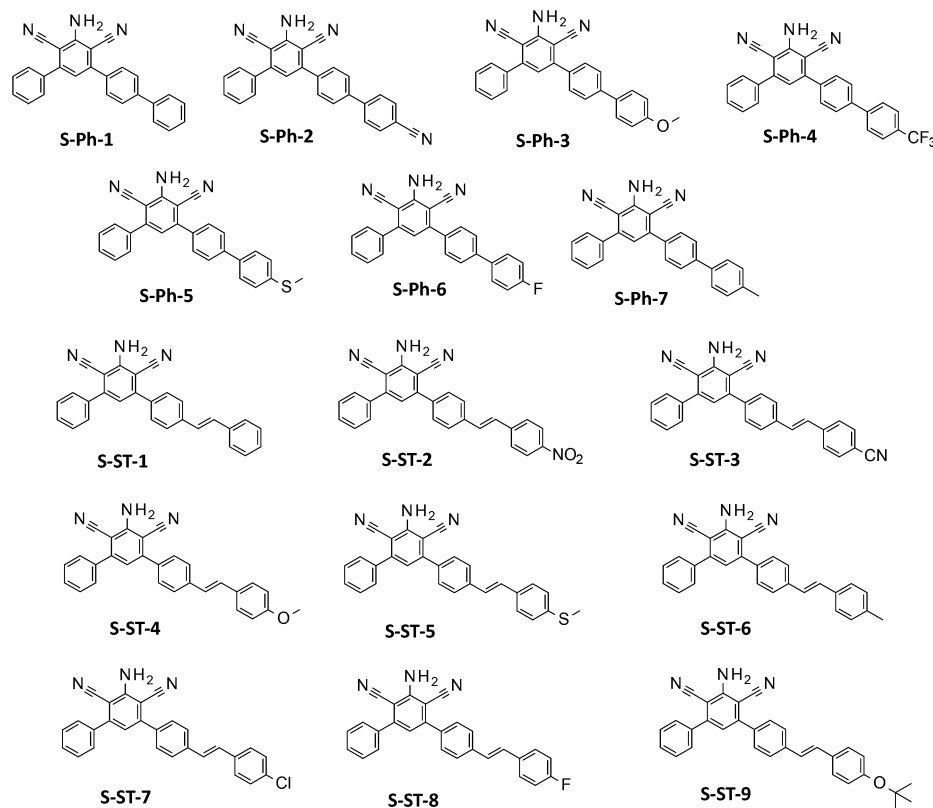


Fig. 1 Structures of the sensors studied.

changes in the reaction environment. These techniques are thus complementary.

The FPT is based on the measurement of changes in the fluorescence characteristics of an appropriate fluorescent sensor (also called a probe), added at a small concentration to the reaction medium. During the polymerization progress, the sensor changes its fluorescence<sup>38,39</sup> or absorbance<sup>40</sup> characteristics as a result of the changes of the system viscosity<sup>41–43</sup> or polarity.<sup>44,45</sup> Thus, the quanta of light emitted by the probe molecules carry information about the changes that occur during the reaction.<sup>46–48</sup> Several different types of fluorescent probes have been developed so far to monitor the polymerization processes. Any process that causes changes in the polarity or microviscosity of the system can be monitored by the FPT, but depending on the nature of the changes, an appropriate selection of the sensor with good sensitivity and emission quantum efficiency is necessary. The limited versatility of already known fluorescent probes makes it still crucial to search for new, more versatile molecules that could be employed as molecular sensors to monitor cationic, free radical and hybrid polymerization processes with the same sensor.

In this paper, we report the applicability of 2-amino-4,6-diphenylbenzene-1,3-dicarbonitrile derivatives as versatile fluorescent molecular sensors for monitoring both cationic and free-radical polymerization processes of various monomers by the Fluorescence Probe Technique (FPT). Moreover, the performance

of those sensors in monitoring the progress of example hybrid photopolymerization processes has been evaluated.

## Experimental procedures

### Materials

Two groups of *meta*-terphenyl derivatives based on a 2-amino-4,6-diphenylbenzene-1,3-dicarbonitrile core (Fig. 1) have been evaluated for their suitability as fluorescent molecular sensors for monitoring photopolymerization processes by the FPT. The sensors in the first group, labelled with an S-Ph prefix, contained an additional substituted phenyl ring at the *para*-position of one of the phenyl rings of the core. These were: 2-amino-4-phenyl-6-(4-phenylphenyl)benzene-1,3-dicarbonitrile (S-Ph-1), 2-amino-4-[4-(4-cyanophenyl)phenyl]-6-phenylbenzene-1,3-dicarbonitrile (S-Ph-2), 2-amino-4-[4-(4-methoxyphenyl)phenyl]-6-phenylbenzene-1,3-dicarbonitrile (S-Ph-3), 2-amino-4-phenyl-6-[4-[4-(trifluoromethyl)phenyl]phenyl]benzene-1,3-dicarbonitrile (S-Ph-4), 2-amino-4-[4-(4-methylsulfanylphenyl)phenyl]-6-phenylbenzene-1,3-dicarbonitrile (S-Ph-5), 2-amino-4-[4-(4-fluorophenyl)phenyl]-6-phenylbenzene-1,3-dicarbonitrile (S-Ph-6), and 2-amino-4-[4-(4-methylphenyl)phenyl]-6-phenylbenzene-1,3-dicarbonitrile (S-Ph-7).

The second group, labelled with an S-ST prefix, was composed of the sensors, where an appropriately substituted styryl group was attached in place of the additional phenyl ring, so



that the phenyl ring was separated with an additional double bond from the *m*-terphenyl core. This series consisted of the following derivatives: 2-amino-4-phenyl-6-[4-[(*E*)-styryl]phenyl]benzene-1,3-dicarbonitrile (S-ST-1), 2-amino-4-[4-[(*E*)-2-(4-nitrophenyl)vinyl]phenyl]-6-phenyl-benzene-1,3-dicarbonitrile (S-ST-2), 2-amino-4-[4-[(*E*)-2-(4-cyanophenyl)vinyl]phenyl]-6-phenyl-benzene-1,3-dicarbonitrile (S-ST-3), 2-amino-4-[4-[(*E*)-2-(4-methoxyphenyl)vinyl]phenyl]-6-phenyl-benzene-1,3-dicarbonitrile (S-ST-4), 2-amino-4-[4-[(*E*)-2-(4-methylsulfanylphenyl)vinyl]phenyl]-6-phenyl-benzene-1,3-dicarbonitrile (S-ST-5), 2-amino-4-[4-[(*E*)-2-(4-methylphenyl)vinyl]phenyl]-6-phenyl-benzene-1,3-dicarbonitrile (S-ST-6), 2-amino-4-[4-[(*E*)-2-(4-chlorophenyl)vinyl]phenyl]-6-phenyl-benzene-1,3-dicarbonitrile (S-ST-7), 2-amino-4-[4-[(*E*)-2-(4-fluorophenyl)vinyl]phenyl]-6-phenyl-benzene-1,3-dicarbonitrile (S-ST-8) and 2-amino-4-[4-[(*E*)-2-(4-*tert*-butoxyphenyl)vinyl]phenyl]-6-phenyl-benzene-1,3-dicarbonitrile (S-ST-9). Structures of the sensors studied are shown in Fig. 1, while their synthesis and  $^{13}\text{C}$ -NMR,  $^1\text{H}$ -NMR and LC-MS analyses were reported in a previous paper.<sup>49</sup>

Commercially available diphenyliodonium hexafluorophosphate (HIP, Alfa Aesar, Haverhill, MA, USA) and 2,2-dimethoxy-2-phenylacetophenone (DMPA, Sigma Aldrich, Hamburg, Germany) were used as the cationic and free-radical photoinitiators, respectively. For cationic photopolymerization, standard monomers such as 3,4-epoxycyclohexylmethyl 3,4-epoxy-cyclohexanecarboxylate (CADE, Lambson Ltd, Wetherby, UK) and triethylene glycol divinyl ether (TEGDVE, Sigma Aldrich) were used, while for free-radical photopolymerization tetraethylene glycol dimethacrylate (TEGDMA, Sigma Aldrich) and tetraethylene glycol diacrylate (TEGDA, Sigma Aldrich) were used. The performance of the sensors studied in the following other monomers or monomer mixtures was also verified: trimethylolpropane triacrylate (TMPTA, Sigma Aldrich) and glycidyl methacrylate (GlyMA, Sigma Aldrich). The structures of the materials used in this study are shown in Fig. 2.

### Absorbance measurements

The absorption spectra were obtained using an EPP2000C spectrometer (StellarNet, Inc., Tampa, FL, USA) with the spec-

tral range 190–850 nm and a broadband deuterium-halogen lamp, emitting in the range of 190–2500 nm. The measurements were carried out in a quartz cuvette with a 1.0 cm optical path at room temperature. The absorbance values were converted to molar extinction coefficients, expressed in the units  $[\text{dm}^3 \text{mol}^{-1} \text{cm}^{-1}]$ .

### Fluorescence measurements

Fluorescence spectra of the sensors studied in different solvents were obtained using the same EPP2000C spectrometer, but in combination with a UV LED and an appropriate adapter. The following UV LEDs were used as the excitation light sources: UV-LED-320 emitting at  $\lambda_{\text{max}} = 320 \text{ nm}$  (UVTOP315-BL-TO39, Roithner Laser Technik GmbH, Austria) and a UV-LED emitting at  $\lambda_{\text{max}} = 365 \text{ nm}$  (Amecam, Warsaw, Poland). The fluorescence spectra were recorded at room temperature (25 °C). All the solvents were of spectroscopic purity.

### FPT measurements

**Preparation of thin-layer samples.** Photo-curable compositions of three components were prepared: a photoinitiator (at a concentration of 1% by weight), a fluorescent molecular probe (*i.e.*, the *meta*-terphenyl derivative at a concentration of 0.1% by weight) and an appropriately selected monomer or mixture of monomers. Due to the photosensitivity of the compositions, the samples were prepared in a dimmed room and were protected from daylight. The thin-layer samples were prepared by placing two drops of the evaluated composition between two microscopic slides (Thermo Scientific, Waltham, MA, USA), which were separated on the sides with 0.1 mm spacers. The slides were clipped together with paper clips to prevent displacement. So the prepared sample was placed horizontally in a temperature-controlled measurement chamber, directly above the UV-LED. The temperature during the measurements was kept constant at 25 °C. The recording of fluorescence spectra was started immediately after placing the sample into the preheated chamber. The measurements were done automatically under computer control, and the data were recorded on the computer configured with the apparatus. A

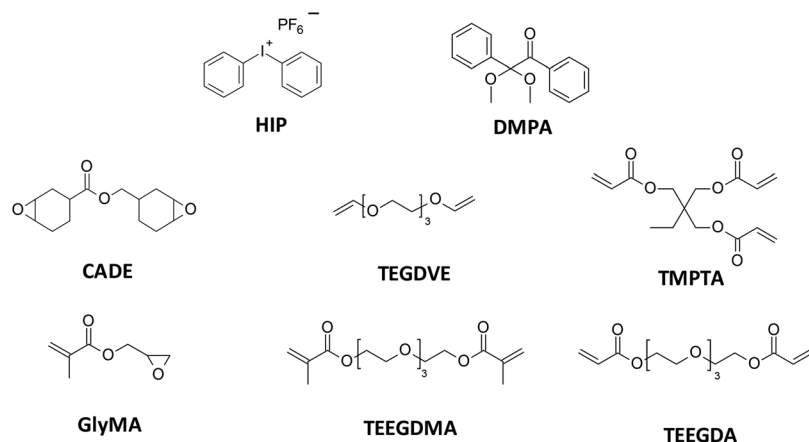
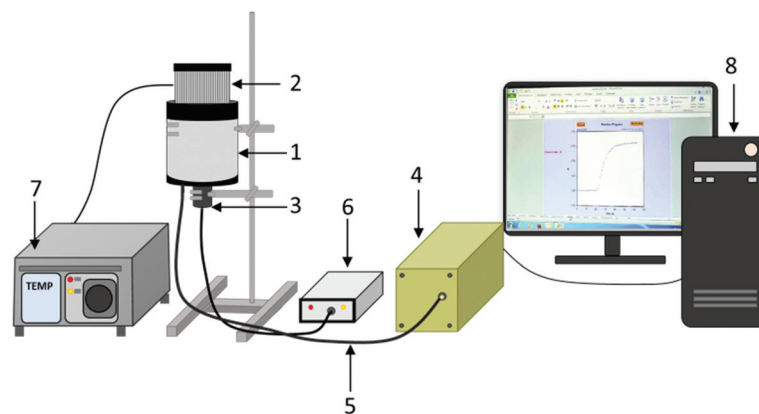


Fig. 2 Structures of the photoinitiators and monomers.





**Fig. 3** Schematic illustration of the FPT equipment. (1 – measurement chamber, 2 – thermostatic head based on a Peltier cell, 3 – sensor head with UV LED, 4 – EPP200C spectrometer, 5 – fiber optic cable with a 2 mm core, 6 – stabilized constant current source (23 mA) for the UV LED, controlled via USB, 7 – ITC4020 temperature controller, 8 – PC computer.)

schematic illustration of the instrumentation used is shown in Fig. 3, while a photograph of a similar measurement setup was published previously.<sup>49</sup>

**Monitoring the progress of photopolymerization processes.** The ratio of fluorescence intensities ( $R$ ), measured at two different wavelengths, located on both sides of the fluorescence spectrum maximum, was used as an indicator of the photopolymerization progress. This parameter increases with the polymerization progress when the spectrum shifts towards shorter wavelengths. The main advantage of this method is the possibility to measure precisely the intensity ratio, which does not depend on the probe concentration or the geometric dimensions of the sample. It is a relative value, which is proportional to the monomer conversion. The ratio ( $R$ ) was defined by eqn (1):<sup>50–53</sup>

$$R = \frac{I(\lambda_1)}{I(\lambda_2)} \quad (1)$$

where  $I(\lambda_1)$  is the fluorescence intensity at a shorter wavelength and  $I(\lambda_2)$  is the fluorescence intensity at a longer wavelength. In order to determine parameter  $R$ , individual wavelengths corresponding to half height of the fluorescence spectrum before photopolymerization were selected for each composition separately.

Additionally, in order to compare quantitatively how the nature and position of the substituents in the probe structure affect the sensitivity of these systems, the relative sensitivity ( $S$ ) parameter was defined by eqn (2):

$$S = \frac{R_a - R_b}{R_b} \times 100\% \quad (2)$$

where  $R_b$  is the ratio before polymerization and  $R_a$  is the final ratio after monomer polymerization.

## Results and discussion

Fluorophores suitable for application as fluorescent molecular sensors have to have appropriate spectral characteristics. In particular, such fluorophores have to exhibit high enough fluo-

rescence intensity at low concentrations, so that the sensor concentration can be maintained as low as possible, while still enabling recording noise-free fluorescence spectra, and the fluorophores have to be very sensitive to minute changes of medium polarity. Both these features depend on the core fluorophore structure and on the type of substituent. Hence, first the basic spectroscopic properties of the fluorophores studied were investigated.

### The influence of the chemical structure on absorption and emission characteristics

The UV-Vis absorption spectra of 2-amino-4,6-diphenylbenzene-1,3-dicarbonitrile derivatives in acetonitrile are presented in Fig. 4. The phenyl-substituted derivatives (S-Ph series) exhibit a long-wavelength absorption band in the range of 340–400 nm, whereas the absorption of styryl-substituted derivatives (S-ST series) is slightly shifted towards longer wavelengths and reaches up to about 450 nm. In addition, the styryl derivatives exhibit a molar extinction coefficient of the long-wavelength absorption band about twice higher than that of the phenyl-substituted derivatives. The observed differences in light absorption between the S-Ph and S-ST series result from more extended conjugation in the latter series due to the presence of an additional double bond.

Quantitative parameters of the absorption spectra are summarized in Table 1. The absorption maximum of the long-wavelength band of the derivatives studied is not affected by the substituents, which is particularly visible in the case of the S-Ph series, where the long-wavelength band is well separated from adjacent absorption bands (Fig. 4a). The absorption maximum of that band for all of the derivatives studied is very close to the emission maximum of easily available commercial UV LEDs, emitting maximum light intensity at 365 nm. This makes those LEDs a good choice as the excitation light sources to maximize the fluorescence intensity of the sensors studied. However, these sensors can be excited also by any other UV light sources emitting at shorter wavelength than the  $\lambda_{\text{max-ab}}$ ,



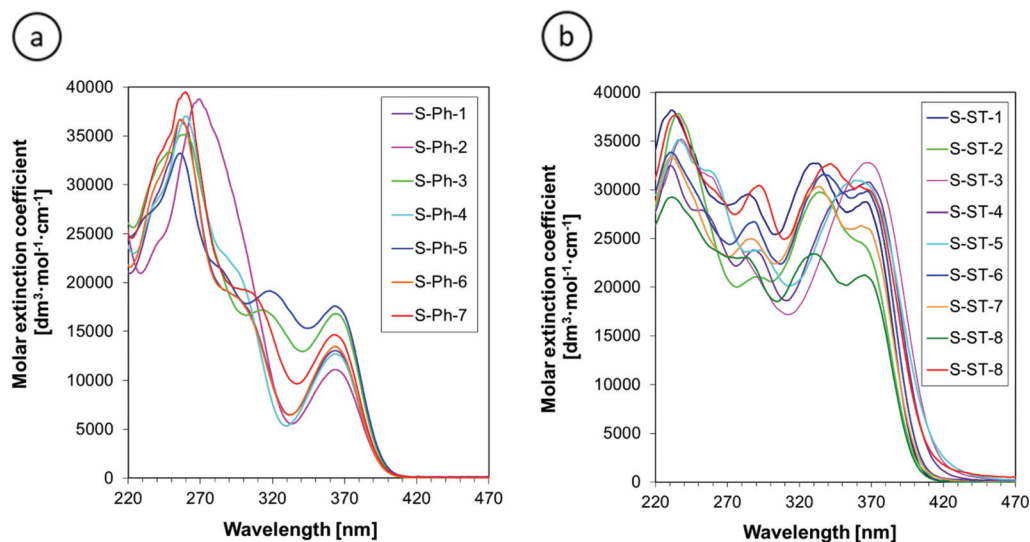


Fig. 4 UV-Vis absorption spectra of: (a) 2-amino-4-phenyl-6-(4-phenylphenyl)benzene-1,3-dicarbonitrile derivatives and (b) 2-amino-4-phenyl-6-[4-((E)-styryl)phenyl]benzene-1,3-dicarbonitrile derivatives, in acetonitrile.

Table 1 Spectroscopic characteristics of the 2-amino-4-phenyl-6-(4-phenylphenyl)benzene-1,3-dicarbonitrile and 2-amino-4-phenyl-6-[4-((E)-styryl)phenyl]benzene-1,3-dicarbonitrile derivatives in acetonitrile

Sensor	Substituent	$\lambda_{\max-ab}^a$ [nm]	$\epsilon_{@ \lambda_{\max-ab}}$ [dm <sup>3</sup> mol <sup>-1</sup> cm <sup>-1</sup> ]	$\lambda_{\max-fl}$ [nm]	$I_{\max-fl}$ [a.u.] ( $\lambda_{exc} = 320$ nm)	$I_{\max-fl}$ [a.u.] ( $\lambda_{exc} = 365$ nm)
S-Ph-1	H	363	13 000	427	1488	1252
S-Ph-2	CN	363	11 100	431	1633	1147
S-Ph-3	OMe	363	16 800	434	1684	1295
S-Ph-4	CF <sub>3</sub>	363	12 700	429	1120	1170
S-Ph-5	SMe	363	17 600	506	1483	1385
S-Ph-6	F	363	13 500	427	1480	1407
S-Ph-7	Me	362	14 600	426	1820	1720
S-ST-1	H	365	28 800	437	2323	1823
S-ST-2	NO <sub>2</sub>	—	—	—	25	115
S-ST-3	CN	360	32 700	433	1905	1846
S-ST-4	OMe	368	30 800	531	1231	1707
S-ST-5	SMe	360	31 000	537	892	1226
S-ST-6	Me	365	29 900	493	2377	2177
S-ST-7	Cl	360	26 300	435	2080	1787
S-ST-8	F	365	21 200	437	1857	1666
S-ST-9	OCMe <sub>3</sub>	360	30 400	538	966	930

<sup>a</sup> Absorption maximum of the long-wavelength absorption band.

because their minimal extinction coefficient at the shorter wavelengths is only less than two-times lower than that at the  $\lambda_{\max-ab}$  (Fig. 4).

Fluorescence spectra of the 2-amino-4,6-diphenyl-benzene-1,3-dicarbonitrile derivatives were measured at two excitation wavelengths  $\lambda_{exc} = 320$  nm and  $\lambda_{exc} = 365$  nm in acetonitrile to compare the advantages and disadvantages of using the particular excitation wavelengths. The fluorescence spectra obtained upon excitation at 320 nm are shown in Fig. 5. The fluorescence spectra recorded at 365 nm excitation had the same shape, but different fluorescence intensity due to different extinction coefficients at the longer excitation wavelength. The fluorescence intensities at different excitation wavelengths but at the same fluorophore concentration are compared in Table 1.

Fig. 5 indicates that all of the derivatives studied, except for S-ST-2, exhibit high enough fluorescence efficiency to record noise-free fluorescence spectra at short data acquisition times, which is important for fluorescent sensors. The derivative S-ST-2 contains a nitro group in its structure. If a nitro group is not conjugated with a strongly electron-donating substituent to enable intramolecular charge transfer in the excited state, the presence of the nitro group in a fluorophore quenches its fluorescence. Consequently, S-ST-2 showed very weak fluorescence and it can be eliminated from the list of candidates for the sensor applications.

The fluorescence peak positions of the *m*-terphenyls studied appear in the range 390–700 nm (Fig. 5). The fluorescence spectra are much more affected by the substituents than the corresponding absorption spectra. Unsubstituted



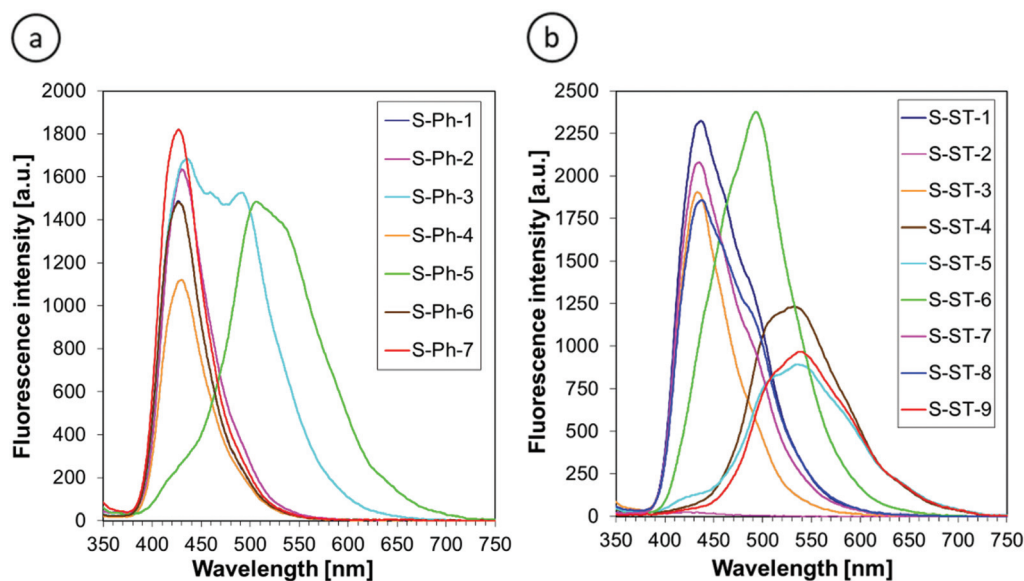


Fig. 5 Fluorescence spectra of (a) 2-amino-4-phenyl-6-(4-phenylphenyl)benzene-1,3-dicarbonitrile derivatives and (b) 2-amino-4-phenyl-6-[4-(*E*-styryl)phenyl]benzene-1,3-dicarbonitrile derivatives in acetonitrile at  $\lambda_{\text{exc}} = 320$  nm.

derivatives (*i.e.*, S-Ph-1 and S-ST-1) and those containing electron-withdrawing substituents (*i.e.*, S-Ph-2, S-Ph-4, S-Ph-6, S-ST-3, S-ST-7 and S-ST-8) emit in the same range of 390–550 nm with the maximum intensity at  $429 \pm 2$  nm for the S-Ph series and  $435 \pm 2$  nm for the S-ST series. On the other hand, electron-donating substituents, such as methoxy (OMe), *t*-butoxy (OCMe<sub>3</sub>), methylsulfanyl (SMe) and methyl (Me) groups shifted the fluorescence spectra to longer wavelengths by several dozen nanometers (Table 1). This can be attributed to a push–pull effect in the excited state between the electron-donating substituents on the phenyl or styryl ring and the electron-withdrawing cyano group at position 1 of the pyridine ring. Strong electron delocalization along the conjugated system in the excited state stabilizes the excited state and lowers its energy, which results in the strong fluorescence spectral shift to longer wavelengths.

Fluorescence intensity is also affected by the type of substituent, but to a lesser extent than the fluorescence peak position. Among the sensors studied (*i.e.*, while neglecting the nitro derivative S-ST-2, which does not qualify for the role of a sensor), S-ST-6 showed the highest fluorescence intensity, while the lowest intensity, observed for S-ST-5 (at 320 nm excitation) or S-ST-9 (at 365 excitation), was only about 2.5-times lower (Table 1).

Finally, comparison of the fluorescence intensities at different excitation wavelengths confirms that in the case of the derivatives studied, the choice of the excitation wavelength is not critical, because the fluorescence intensities measured for the same compounds at 320 nm and 365 nm excitation are similar (Table 1). Hence, for practical applications a 320 nm UV LED will be better as the excitation light source, because we noticed that in the case of a 365 nm LED, the excitation light scattered by the sample slightly overlapped with the fluorescence spectra at the short wavelength side.

### The performance of the sensors studied in polymerizing media

**Applicability of the *m*-terphenyls as fluorescent sensors for monitoring cationic photopolymerization of monomers.** The major advantage of cationic photopolymerization is the fact that it is not inhibited by oxygen present in air, and once started, it continues even after the light has been switched-off. Moreover, the possibility of performing the polymerization process at ambient temperature makes the preparation of polymeric materials by photoinduced cationic polymerization one of the most efficient photochemical techniques. The dynamic progress in the development of this type of photopolymerization is also due to expanding assortment of monomers polymerized by the cationic mechanism. Usually, vinyl ethers and epoxy monomers are polymerized by cationic photopolymerization. These monomers show lower toxicity in comparison with traditional compositions based on acrylic monomers.<sup>54</sup> In particular, vinyl ethers show high reactivity. Therefore, the performance of the sensors studied in triethylene glycol divinyl ether (TEGDVE) as a model monomer was evaluated first. Commercially available diphenyliodonium hexafluorophosphate (HIP, 1.0 wt%) was used as the cationic photoinitiator. The quantity of the sensor was 0.1% by weight, which was equivalent to the molar concentration of  $2.1 \times 10^{-3}$ – $2.7 \times 10^{-3}$  mol dm<sup>-3</sup>, depending on the sensor molecular weight. *trans*-2-(2′5′-Dimethoxyphenyl)ethenyl-2,3,4,5,6-pentafluorobenzene (25ST) was used as a reference sensor for comparison. The same UV LED, emitting at 320 nm, was used as the light source for inducing the monomer photopolymerization and excitation of the probe. The fluorescence spectra of example sensors at various photopolymerization times of the TEGDVE monomer are shown in Fig. 6, while the



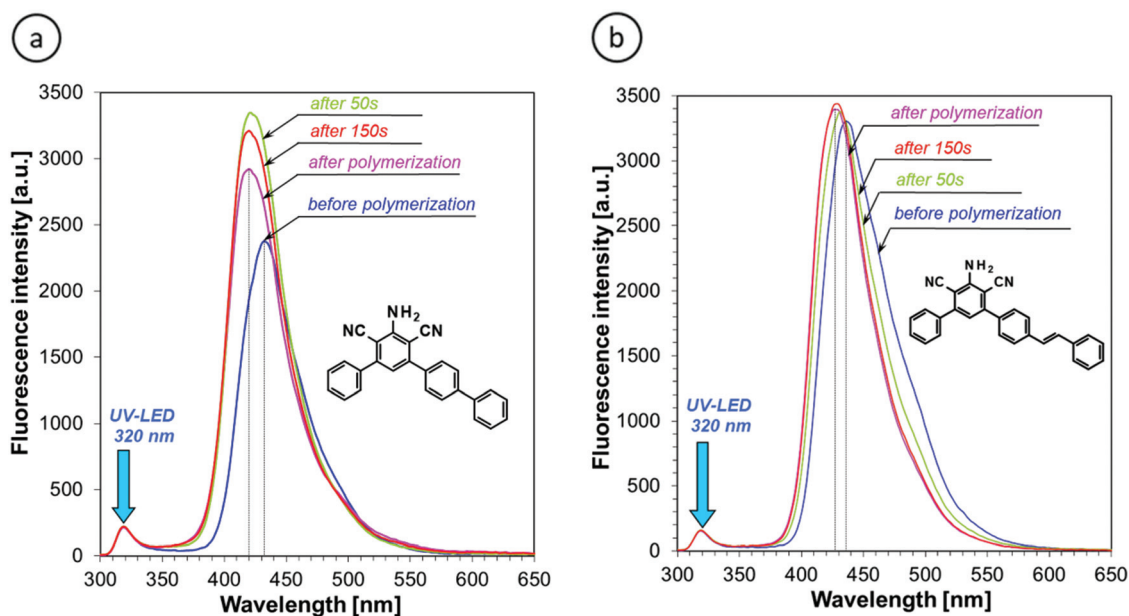


Fig. 6 Changes of the emission spectra of (a) S-Ph-1 and (b) S-ST-1 upon cationic photopolymerization of the TEGDVE monomer.

changes of the spectral position, fluorescence intensity and sensitivity ( $S$ ) of all of the sensors studied are summarized in Table 2.

The fluorescence spectra of all of the derivatives studied, except for S-ST-2, shifted towards shorter wavelengths (Fig. 6 and Table 2). The largest shift was observed for SMe-substituted sensors in both sensor series, and the alkoxy-substituted sensors in the S-ST series (Table 2). Hence, the derivatives substituted with the electron-donating substituents show the highest sensitivity to polarity changes occurring during cationic photopolymerization of the TEGDVE monomer. This is consistent with the push-pull effect discussed in the previous

section and indicates that strong electron delocalization in the excited state is critical for high sensitivity of a sensor to polarity changes. Nevertheless, all of the derivatives studied (*i.e.*, except for S-ST-2) shifted their fluorescence spectrum more than the 25ST reference, which so far has been used as one of the few sensors known, suitable to study cationic photopolymerization processes. This means that all of the *m*-terphenyls studied show high enough sensitivity to be used as sensors for the cationic polymerization processes.

The fluorescence intensity of the sensors studied, measured at the peak maximum, was only slightly affected by the monomer polymerization (*i.e.*, by less than 50%, except for

Table 2 Changes of fluorescence characteristics of the sensors studied upon cationic photopolymerization of the TEGDVE monomer

Sensor	Substituent	$\lambda_{\text{max-b}}$ [nm]	$I_{\text{max-b}}$ [a.u.]	$\lambda_{\text{max-a}}$ [nm]	$I_{\text{max-a}}$ [a.u.]	$\Delta\lambda_{\text{max}}$ [nm]	$S$ [%]	$\Delta I/I_b$ [%]
S-Ph-1	H	432	1426	420	1752	-12	169	23
S-Ph-2	CN	437	1109	425	1580	-12	219	42
S-Ph-3	OMe	433	1775	420	2044	-13	179	15
S-Ph-4	CF <sub>3</sub>	435	1091	421	1493	-14	184	37
S-Ph-5	SMe	493	1402	425	2087	-67	1440	49
S-Ph-6	F	432	1498	419	1892	-13	174	26
S-Ph-7	Me	432	1733	419	2048	-12	166	18
S-ST-1	H	436	1984	427	2038	-9	183	3
S-ST-2	NO <sub>2</sub>	434	44	434	249	—	—	466
S-ST-3	CN	440	2616	428	2846	-12	230	9
S-ST-4	OMe	501	2357	440	2264	-60	546	4
S-ST-5	SMe	501	1783	461	1917	-39	515	7
S-ST-6	Me	453	2722	430	3115	-23	563	14
S-ST-7	Cl	438	3360	429	3435	-8	169	2
S-ST-8	F	437	3191	427	3165	-9	198	1
S-ST-9	OCMe <sub>3</sub>	501	2111	440	1828	-61	537	13
25ST	(Reference)	440	785	433	844	-7	159	8

Indexes "b" and "a" denote the data before polymerization and after polymerization, respectively;  $\Delta\lambda_{\text{max}}$  is the shift of the fluorescence spectrum upon monomer polymerization ( $\Delta\lambda_{\text{max}} = \lambda_{\text{max-a}} - \lambda_{\text{max-b}}$ ),  $S$  is the sensor sensitivity defined by eqn (2), and  $\Delta I/I_b$  is the corresponding relative change of fluorescence intensity in [%] ( $\Delta I/I_b = (I_{\text{max-a}} - I_{\text{max-b}})/I_{\text{max-b}} \times 100\%$ ).



S-ST-2, Table 2). For most of the sensors, the fluorescence intensity increased. This is a typical behavior of fluorescent molecular sensors in polymerizing media, which comes from the fact that upon rigidification of the sensor environment, the radiationless excitation energy dissipation into vibrational energy levels of the molecule becomes less efficient due to the inhibition of molecule free movements. Interestingly, the S-ST-2 derivative that showed too low fluorescence intensity in acetonitrile and in a liquid TEGDVE monomer to be useful as a sensor at low monomer conversions increased the fluorescence intensity more than 4-times upon monomer polymerization. This means that the fluorescence intensity of S-ST-2 is highly sensitive to changes of medium microviscosity, while being little affected by changes of the medium polarity. Hence, the nitro-substituted derivative (S-ST-2) may be considered for application as a sensor of minute changes in polymer rigidity, occurring in the final stages of polymerization processes, or for example upon polymer aging.

Either the fluorescence spectrum shift or changes of the fluorescence intensity can be used for monitoring the progress of polymerization processes. For the purpose of this research, we selected the ratio method, defined in the Experimental section, because it is more accurate and independent of geometrical measurement parameters. Fig. 7 shows the photopolymerization profiles, obtained by FPT using the sensors studied.

Fig. 7 confirms that the sensors that showed the highest shift of their fluorescence spectrum upon TEGDVE polymerization (Table 2) also showed the highest ratio span between the unpolymerized and polymerized states of the monomer. However, the ratio span is large enough for all of the sensors studied to be measured precisely and it is even higher than that of the 25ST reference probe. Hence, where sensitivity is concerned, all of the derivatives studied (*i.e.*, except for S-ST-2) are sensitive enough to be used as fluorescent molecular

sensors for monitoring the progress of cationic polymerization processes by FPT, using the fluorescence intensity ratio ( $R$ ) as the progress indicator. However, a closer look at Fig. 7a reveals that some of the sensors in the S-Ph series have limitations. That is, the sensors in this series showed a slight decrease of the ratio ( $R$ ) upon prolonged irradiation. This does not mean that the degree of monomer polymerization decreased; it is just an artifact resulting from slow photolysis of the sensor. When one of the photolysis products is fluorescent and emits at a longer wavelength than the sensor itself, an overlap of the fluorescence spectrum of the side product with the spectrum of the sensor at the long wavelength side causes an apparent increase of the intensity  $I(\lambda_2)$  that results in a gradual decrease of the ratio ( $R$ ) in time, when the polymerization is over. Interestingly, in the case of the S-ST series of sensors no disturbance of the curing profiles was observed (Fig. 7b). Therefore, the S-Ph series of sensors will be more suitable for monitoring rapid cationic polymerization processes, where the sensor photolysis effect is negligible, while the S-ST series can be expected to be suitable also for slowly polymerizing systems.

**Applicability of the *m*-terphenyl derivatives as fluorescent sensors for free-radical photopolymerization processes.** Free-radical polymerization processes are extremely important in the chemical industry due to a large number of available monomers that undergo this type of reaction. Hence, the performance of the derivatives studied as sensors for monitoring free-radical polymerization processes has also been tested. Tetraethylene glycol diacrylate (TEGDGA) and tetraethylene glycol dimethacrylate (TEGDMA) were selected as model monomers polymerizing by the free-radical polymerization mechanism and 2,2-dimethoxy-2-phenylacetophenone (1.0 wt%) was used as a typical free-radical photoinitiator. The sensor concentration was the same as that used for cationic polymerization processes. The kinetic profiles of the free-

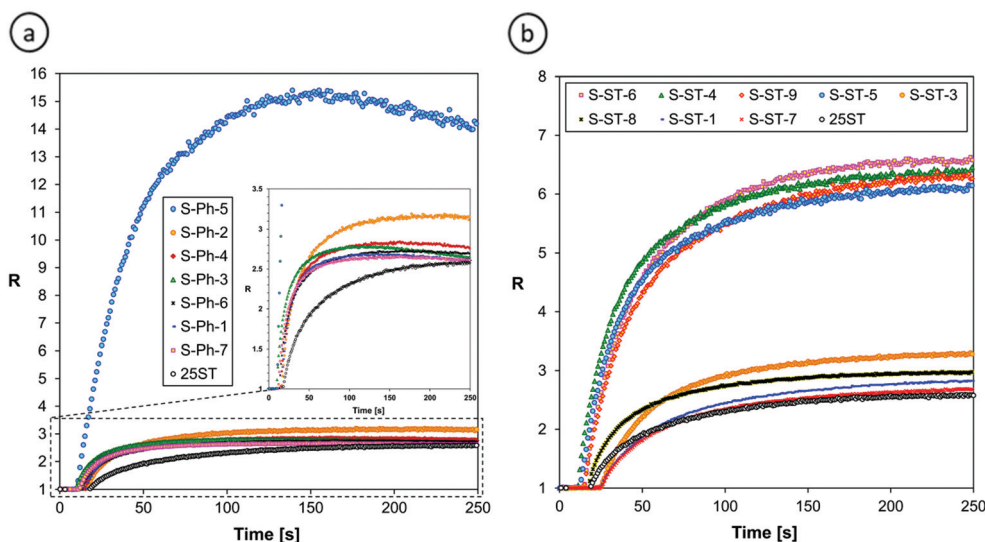
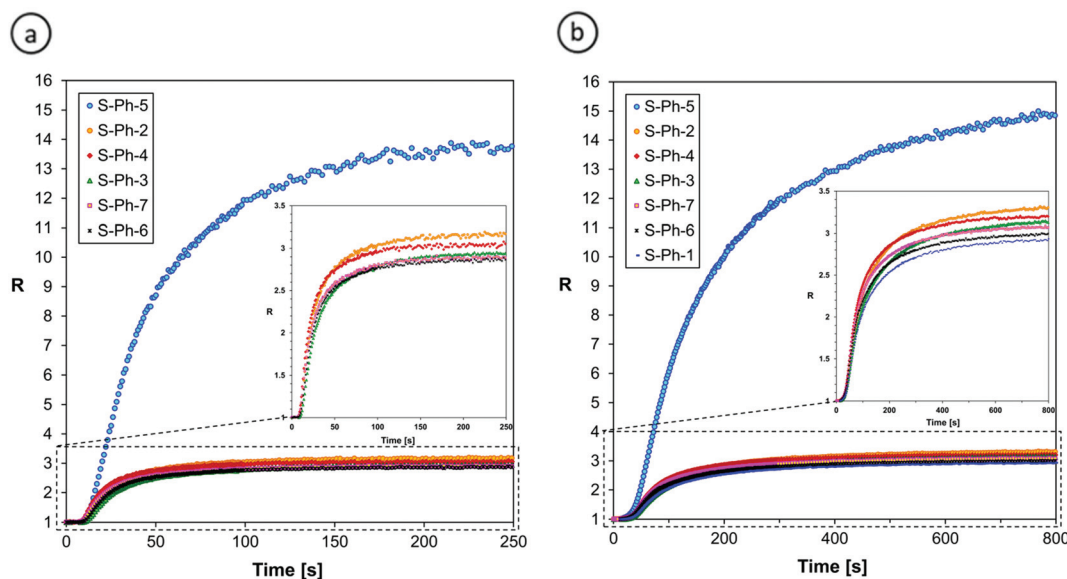


Fig. 7 Monitoring the progress of cationic photopolymerization of the TEGDVE monomer using (a) S-Ph and (b) S-ST series of the sensors studied.





**Fig. 8** Monitoring the progress of free radical photopolymerization of (a) TEEGDA and (b) TEEGDMA using 2-amino-4-phenyl-6-(4-phenylphenyl)benzene-1,3-dicarbonitrile derivatives, at a 320 nm irradiation wavelength.

radical photopolymerization of the acrylic monomers, upon exposure to 320 nm light from a UV LED, using the sensors from the S-Ph series, are shown in Fig. 8, while quantitative parameters of the sensor response during the free radical polymerization are presented in Table 3.

Fig. 8 indicates that all of the S-Ph sensors perform well in monitoring the progress of free radical polymerization processes. Regular photopolymerization profiles have been obtained without any artefacts, even though in the case of free radical polymerization, the fluorescence intensity of the sensors studied slightly decreased (except for S-Ph-5), probably due to some side reaction of the sensors with the free radicals involved in the polymerization process (Table 3). The diacrylate monomer (TEEGDA) polymerized faster than the dimethacrylate monomer (TEEGDMA), as indicated by about three times

shorter irradiation time required to reach a plateau in the curing profiles of TEEGDA compared to those of TEEGDMA (Fig. 8). This comes from a lower propagation rate constant of the addition of methacrylate functional groups to growing macroradicals, compared to the addition of acrylates, due to higher steric hindrance in the case of tertiary methacrylate-terminated macroradicals, compared to secondary acrylate-terminated macroradicals.

The relative increase of the fluorescence intensity ratio upon monomer polymerization, defined as the sensor sensitivity ( $S$ ) by eqn (2), exceeded 100%, which is high enough to measure the progress of free radical polymerization precisely (Table 3). The sensor S-Ph-5, containing a methylsulfanyl substituent, is exceptional in the S-Ph series. Its sensitivity to changes in its environment during free radical polymerization

**Table 3** Changes of fluorescence characteristics of 2-amino-4-phenyl-6-(4-phenylphenyl)benzene-1,3-dicarbonitrile derivatives upon photopolymerization of TEEGDA and TEEGDMA monomers

Sensor	Substituent	$\lambda_{\max-b}$ [nm]	$I_{\max-b}$ [a.u.]	$\lambda_{\max-a}$ [nm]	$I_{\max-a}$ [a.u.]	$\Delta\lambda_{\max}$ [nm]	$S$ [%]	$\Delta I/I_b$ [%]
<b>Free-radical photopolymerization of TEEGDA</b>								
S-Ph-1	H	431	3734	418	1976	-13	135	-47
S-Ph-2	CN	435	3220	422	2182	-14	216	-32
S-Ph-3	OMe	432	3749	420	2930	-12	194	-22
S-Ph-4	CF <sub>3</sub>	435	2242	421	1703	-14	203	-24
S-Ph-5	SMe	490	2568	424	3163	-66	1260	23
S-Ph-6	F	432	2922	419	2346	-13	187	-20
S-Ph-7	Me	431	2525	418	1844	-13	189	-27
<b>Free-radical photopolymerization of TEEGDMA</b>								
S-Ph-1	H	431	2094	418	1533	-14	192	-27
S-Ph-2	CN	436	3202	422	2330	-14	230	-27
S-Ph-3	OMe	431	3991	419	2758	-12	214	-31
S-Ph-4	CF <sub>3</sub>	435	2816	420	1579	-15	220	-44
S-Ph-5	SMe	440	4125	421	3752	-19	1390	-9
S-Ph-6	F	432	2414	418	1425	-14	199	-41
S-Ph-7	Me	431	3194	417	1991	-15	207	-38



of monomers is much higher than the sensitivity of the other sensors. This means that the S-Ph-5 sensor can be used in cases where extremely high sensitivity is required, for example, for tracing postcure processes occurring in the dark after photopolymerization, or changes occurring in polymers upon aging. In these applications, using the fluorescence intensity ratio ( $R$ ) as an indicator of the changes is an additional advantage of the S-Ph-5 sensor, compared to S-ST-2, because the ratio  $R$  does not depend on the geometrical factors of the sample, so the sample may be moved between consecutive long-term measurements. Moreover,  $R$  does not depend on the changes of excitation light intensity that may cause errors in measurements. However, in the case of monitoring the entire polymerization processes starting from a monomer and ending in a polymer, too high sensor sensitivity is not necessarily an advantage, because when the fluorescence spectrum of a sensor shifts too much, the intensity at the shorter wavelength may pass through a maximum and start decreasing before the polymerization is complete. Then the relationship between the fluorescence intensity ratio ( $R$ ) and the functional group conversion may become highly non-linear, which may complicate the interpretation of the curing profiles.

**Monitoring the progress of hybrid photopolymerization processes.** There are a lot of other fluorescent molecular sensors applicable for monitoring purely free radical polymerization and at least several known sensors are suitable for cationic polymerization processes. The versatility of the *m*-terphenyl sensors is desired in particular for studying hybrid polymerization, where polymerization according to two different mechanisms occurs simultaneously. Hence, we decided to test the performance of one of the sensors studied in a few example hybrid photopolymerization processes.

Glycidyl methacrylate (GlyMA, Fig. 2) is a bifunctional monomer containing an epoxy group capable of cationic (but not free radical) polymerization, and a methacrylate group capable of free radical (but not cationic) polymerization. Depending on the initiator type, different linear polymer structures can be obtained from the same GlyMA monomer. Moreover, when both cationic and free radical initiators are used simultaneously, or when initiating radicals and cations are generated simultaneously from the same initiator, a hybrid polymerization is possible, where a crosslinked three-dimensional polymer network can be obtained by two parallel mechanisms. Hence, from the same GlyMA monomer three different polymers of different properties can be synthesized. On the other hand, it is well known that diaryliodonium and triarylsulfonium photoinitiators are capable of initiation of both free radical and cationic polymerization processes. So, first we selected a GlyMA monomer in combination with different photoinitiators to test whether the *m*-terphenyl derivatives would distinguish between purely free radical and hybrid photopolymerization processes. The sensor S-Ph-1 was selected for that purpose. The results are shown in Fig. 9.

Fig. 9 indicates that the free radical polymerization of the GlyMA monomer, initiated with a typical free radical photoinitiator, 2,2-dimethoxy-2-phenylacetophenone, was faster

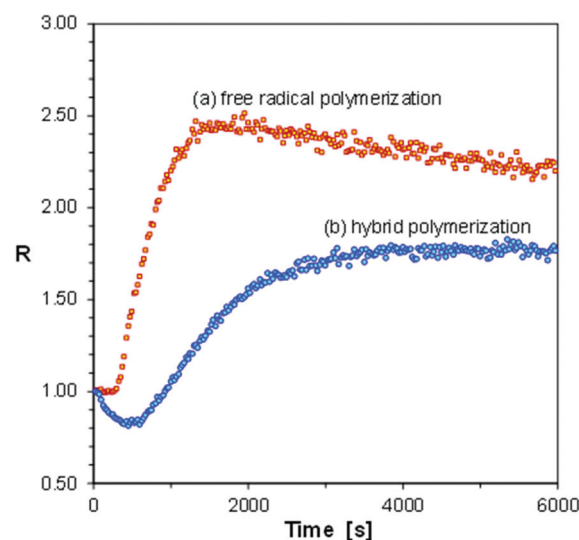


Fig. 9 Photopolymerization profiles of glycidyl methacrylate (GlyMA), obtained by FPT using S-Ph-1 as a fluorescent sensor, in the presence of 2,2-dimethoxy-2-phenylacetophenone (a) or diphenyliodonium hexafluorophosphate (b) as photoinitiators, at a 320 nm irradiation wavelength.

than the corresponding hybrid photopolymerization, initiated with diphenyliodonium hexafluorophosphate, at the same molar concentration of the photoinitiators. This comes from the higher extinction coefficient of the former photoinitiator than that of the latter one at the excitation wavelength. However, in the case of free radical polymerization of GlyMA, a regular curing profile was obtained, while in the case of the hybrid photopolymerization, the fluorescence intensity ratio ( $R$ ) of the S-Ph-1 sensor initially went down to reach a minimum and then increased to a plateau when the polymerization was over (Fig. 9). Moreover, a characteristic short induction period was observed in the case of free radical polymerization, while in the case of hybrid polymerization the ratio changes started immediately after starting irradiation with UV light. This indicates that in the case of the diphenyliodonium photoinitiator, the cationic polymerization of the epoxy groups of GlyMA started immediately, causing an initial decrease of the ratio ( $R$ ), while the free radical polymerization started later on, when the traces of inhibitors present in the monomer (including dissolved oxygen) were used up. As the ratio span caused by free radical polymerization is much higher than that caused by cationic polymerization, after the free radical polymerization induction period, both polymerization types occurred in parallel, but the ratio change was dominated by the ratio increase caused by the free radical polymerization. For example, the fluorescence spectrum of the S-Ph-1 sensor would slightly shift towards longer wavelengths, causing a decrease of the fluorescence intensity ratio during the initial purely cationic polymerization period, where the free radical polymerization mode was yet inhibited. What is noteworthy is that the ratio span between the minimum and maximum values is higher in the case of purely free radical polymerization.



ation of GlyMA than that achieved in the case of hybrid polymerization (Fig. 9). This can be explained by the fact that there is only one methacrylic group per GlyMA molecule. Hence, purely free radical polymerization of the GlyMA monomer leads to a linear polymer that can be called glycidyl poly(methacrylate), where the polymerized methacrylic groups form the polymer main chain, while the glycidyl groups are pending. Monofunctional monomers can be polymerized with even up to 100% monomer conversion. On the other hand, in the case of hybrid polymerization, GlyMA behaves as a bifunctional monomer that forms a crosslinked poly(glycidyl methacrylate) polymer network, where glycidyl poly(methacrylate) chains are crosslinked with poly(glycidyl) methacrylate segments (or *vice versa*). Bifunctional monomers never polymerize to 100% conversion of the functional groups, unless the groups are separated by a long flexible spacer. Similar hybrid photopolymerization of the GlyMA monomer, but initiated with triarylsulfonium salts, was reported previously by Abadie *et al.*<sup>54</sup>

A second example of hybrid polymerization is a simultaneous polymerization of a mixture of a multifunctional monomer, polymerizable only by free radical polymerization, with another multifunctional monomer, polymerizable only by a cationic polymerization mechanism. Such hybrid polymerization leads to interpenetrating polymer networks (IPN), where one crosslinked polymer network, formed by one polymerization mechanism, is incorporated within another polymer network formed by another polymerization mechanism, while the component networks are not linked together by chemical bonds. We selected trimethylolpropane triacrylate (TMPTA) as the free radical monomer and 3,4-epoxycyclohexylmethyl 3,4-epoxy-cyclohexanecarboxylate (CADE) as the monomer polymerizing only by cationic polymerization. Diphenyliodonium hexafluorophosphate (HIP) was selected as the photoinitiator, because it generates both free radical and cationic species capable of simultaneous initiation of free radical and cationic polymerization processes upon irradiation with 320 nm (or shorter) wavelengths of UV light.

Fig. 10 shows the photopolymerization profiles obtained by FPT, using the S-Ph-1 sensor, at various contents of TMPTA in TMPTA/CADE monomer mixtures. Comparison of the profiles obtained for pure CADE and pure TMPTA monomers indicates that the S-Ph-1 sensor is much less sensitive to changes occurring during cationic polymerization of CADE than those occurring during free radical polymerization of TMPTA. However, the ratio span between the cured and uncured states of CADE is still large enough to be monitored by FPT. The ratio span of the TMPTA/CADE mixtures between the cured and uncured states increased with an increase of the TMPTA content. This indicates that also the contents of poly(TMPTA) in the interpenetrating network increased proportionally and confirms that the free radical and cationic photopolymerization processes occurred simultaneously, though not necessarily at the same rate.

In order to take a closer look at the composition of the IPN polymer after photopolymerization, in Fig. 11 we have plotted the final fluorescence intensity ratio ( $R_{\max}$ ), corresponding to

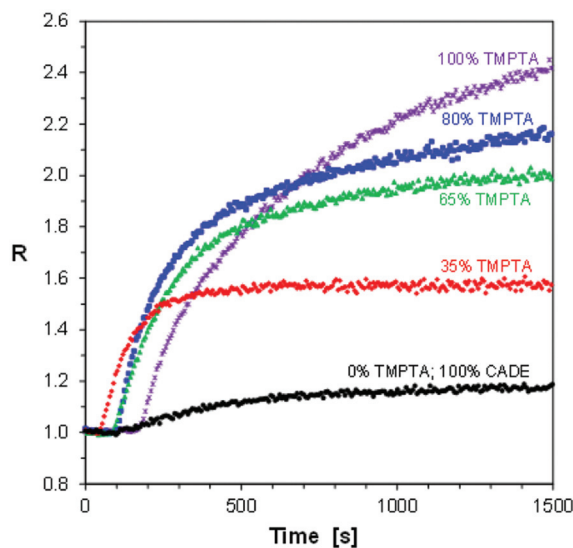


Fig. 10 Progress of hybrid photopolymerization of TMPTA/CADE compositions at various contents of TMPTA monomer (expressed in % by weight), monitored by FPT, using S-Ph-1 as the fluorescent sensor.

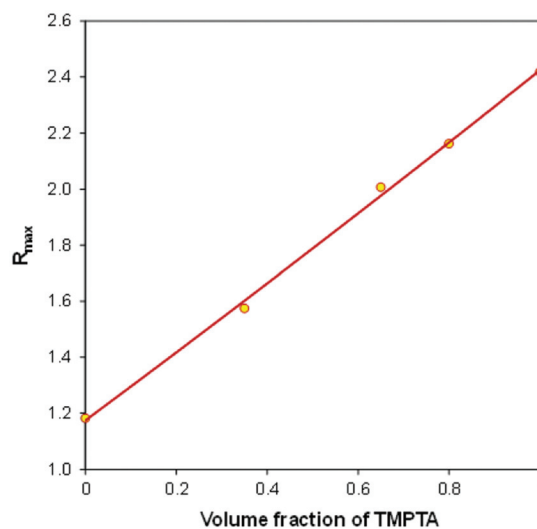


Fig. 11 The relationship between the final fluorescence intensity ratio ( $R_{\max}$ ), achieved after photopolymerization, and the initial composition of a TMPTA/CADE monomer mixture.

1500 s of irradiation time, as a function of the volume fraction of TMPTA in the TMPTA/CADE monomer mixtures.

It can be noticed that in the case of the TMPTA/CADE system the  $R_{\max}$  is linearly proportional to the volume fraction of TMPTA in the monomer mixture. The relationship can be described by the following eqn (3):

$$R_{\max} = R_{\max\text{-pureCADE}} + (R_{\max\text{-pureTMPTA}} - R_{\max\text{-pureCADE}})\phi_{\text{TMPTA}} \quad (3)$$

where  $R_{\max}$  is the fluorescence intensity ratio achieved after hybrid polymerization of the TMPTA/CADE mixture containing



a  $\varphi_{\text{TMPTA}}$  volume fraction of the TMPTA monomer, while  $R_{\text{max\_pureCADE}}$  and  $R_{\text{max\_pureTMPTA}}$  are the final ratios achieved after the polymerization of pure monomers under the same polymerization conditions.

The linearity of the relationship between the fluorescence intensity ratio ( $R_{\text{max}}$ ) and the mixture composition proves that each monomer polymerized independently of the other one. Moreover, it means that during the hybrid polymerization of TMPTA/CADE mixtures, each monomer polymerized with the same conversion as it would in its pure form, causing an overall change of the medium micropolarity proportional to its content. If it was not so and if, for example, in the mixture, one of the monomers polymerized with higher conversion than in its pure state, the contribution of that monomer to the overall polarity change of the mixture would be higher and the relationship would not be linear.

The third example of the hybrid polymerization we decided to study by the FPT, using S-Ph-1 as an example versatile sensor, was the most complex one. It was a hybrid copolymerization of the CADE monomer with glycidyl methacrylate (GlyMA). Both monomers contain epoxy groups capable of undergoing cationic polymerization or copolymerization, while the GlyMA monomer additionally contains a methacrylic group capable of free radical polymerization. The epoxy groups in CADE are more strained due to their location directly on the cyclohexane rings (Fig. 2). Therefore, the CADE monomer usually polymerizes faster by cationic polymerization than any epoxy monomer based on glycidyl functionalities. However, the reactivity difference between the epoxy groups in CADE and GlyMA is not as high as, for example, between epoxy groups and vinyl ether groups to prevent their cationic copolymerization. Hence, one can expect that the hybrid copolymerization of CADE/GlyMA mixtures will form a peculiar polymer network, composed of a crosslinked poly(CADE-*co*-Gly) methacrylate backbone, formed by the cationic copolymerization, additionally crosslinked with poly(methacrylate) segments, formed by free radical polymerization of the methacrylic groups. So, it was interesting to see whether any valuable information about the hybrid copolymerization reaction can be deduced from FPT results. The photopolymerization profiles obtained for different compositions of CADE/GlyMA mixtures (expressed in % by weight) are shown in Fig. 12.

The hybrid photopolymerization of CADE/GlyMA monomer mixtures behaves differently from that of CADE/TMPTA. At high GlyMA contents (*i.e.*, 65% and 80% of GlyMA), the curing profiles showed a period below the initial  $R$  value, characteristic of hybrid polymerization of the pure GlyMA monomer (Fig. 9). However, the magnitude of the  $R$  values that was below the initial value quickly decreased with the increase of CADE contents, and at about 1 : 1 mass ratio of GlyMA/CADE (*i.e.*, at 50% of GlyMA that corresponds to about 64 mol% of GlyMA), only values above the initial value are observed. This indicates that rapid cationic copolymerization of the CADE monomer with glycidyl groups of GlyMA started at the initial stages of the hybrid copolymerization, before the large ratio increase caused by free radical polymerization of methacrylic

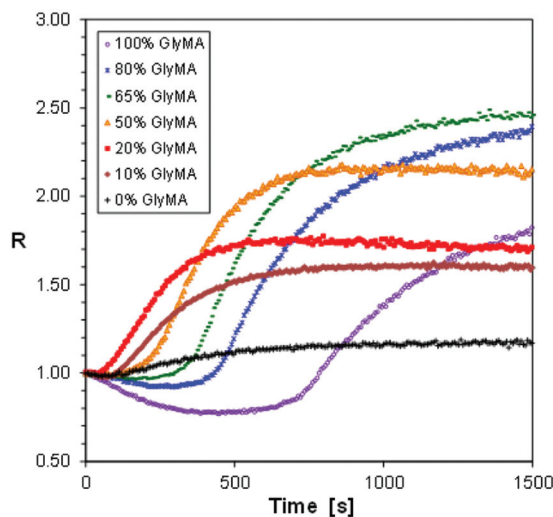


Fig. 12 Photopolymerization profiles of CADE/GlyMA monomer mixtures, initiated with diphenyliodonium hexafluorophosphate under 320 nm UV light.

groups of GlyMA started dominating. The final ratio ( $R_{\text{max}}$ ), achieved after 1500 s of the photopolymerization, initially increased with the increase of GlyMA contents, reached a maximum at about 65% of GlyMA and then slightly decreased (Fig. 12). This means that the overall conversions of both epoxy and methacrylic groups in the copolymers were higher than those in the corresponding homopolymers.

Fig. 13 shows the relationship between the final ratio ( $R_{\text{max}}$ ) and the GlyMA contents in CADE/GlyMA mixtures, in the same coordinate system as that used previously for the TMPTA/

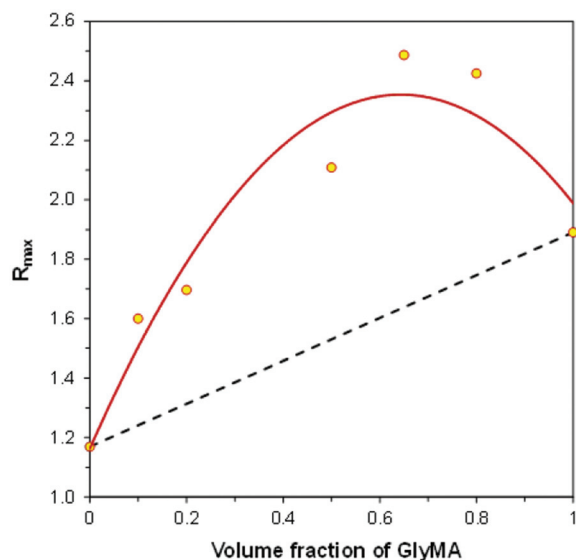


Fig. 13 The relationship between the final fluorescence intensity ratio ( $R_{\text{max}}$ ), achieved after hybrid photopolymerization and the initial composition of the GlyMA/CADE monomer mixture.



CADE compositions. In the case of CADE/GlyMA the relationship is not linear. The broken line in Fig. 13 represents the ratio ( $R_{\max}$ ) that would be achieved if the CADE and GlyMA monomers polymerized independently, as in the case of TMPTA/CADE compositions. Higher  $R_{\max}$  ratios achieved after photopolymerization of CADE/GlyMA mixtures than those calculated from eqn (3) indicate that higher overall conversions of the reactive functional groups present in monomers (*i.e.*, both the epoxy and methacrylic groups) were achieved in the case of mixtures compared to the homopolymerization of pure monomers. This is an important observation, because it is well known that multifunctional monomers do not polymerize with 100% conversion of reactive functional groups. Residues of non-polymerized functional groups may cause problems, in particular in the case of photocurable polymer coatings. For example, unsaturated bonds, left in a polymer coating after polymerization, decrease stain resistance of the coating, because double bonds are more polar and show stronger interaction with environmental contaminants (including dyes) than saturated bonds formed upon polymerization. On the other hand, when residual double bonds in a polymer coating are located at alpha-positions relative to some carbons attached to hydrogen atoms (*e.g.*, to methyl, methylene or methine groups), the coating becomes susceptible to allylic oxidation in air, which causes faster aging of the coating and lowers its durability.

The linearity of the relationship shown in Fig. 11 and strong deviation from linearity observed in Fig. 13 also shed light on how fluorescent molecular sensors respond to changes occurring in their environment during hybrid polymerization processes. That is, what is measured by the FPT and indicated by the change of the fluorescence intensity ratio ( $\Delta R$ ) is the average polarity change that contains contributions resulting from the polymerization of particular types of functional groups. Dipole-dipole interactions that are responsible for the shift of the sensor fluorescence spectrum along the wavelength scale are very short-range interactions, because it is well known that the dipole-dipole interaction energy is inversely proportional to the third power of the distance between interacting dipoles and quickly decays to zero with the distance increase. A single excited sensor molecule may sense no more than one (or possibly maximum two) closest dipoles or polarized bonds. If it is assumed that the sensor molecules are distributed uniformly within the entire volume of the material, some sensor molecules are located in the vicinity of one type of functional group, while the other ones are located in the vicinity of other types of functional groups in monomers or polymer. Hence, what is observed as the sensor response is the average response from the entire population of the sensor molecules interacting with different functional groups. In such cases, the relative sensor response ( $\Delta R$ ), measured as the ratio increase (or decrease), relative to its initial value before polymerization (*i.e.*,  $\Delta R = R - R_b$ ), is the volume average of the relative responses of the sensor molecules to conversions of different types of functional groups located in their vicinity, proportionally to the monomer con-

tents, which in the case of a two-monomer system can be expressed by eqn (4).

$$\Delta R = \Delta R_1 \cdot \varphi_1 + \Delta R_2 \cdot \varphi_2 \quad (4)$$

where  $\Delta R_i$  ( $i = 1$  or  $2$ ) is the ratio changes that would be caused by the polymerization of the same amounts of particular functional groups in pure monomers, and  $\varphi_1$  and  $\varphi_2$  are the volume fractions of the monomers in the initial monomer mixture. Moreover, as the polarity of a medium is proportional to the number of dipoles (*i.e.*, both permanent and induced dipoles) per unit volume, while particular monomers occupy different partial volumes within the mixture, the overall polarity of a mixture can be expected to be proportional to the volume fractions of the components ( $\varphi_i$ ) rather than, for example, to molar fractions.

There is some evidence that when the monitoring wavelengths used in the FPT for measurement of the ratio ( $R$ ) are selected so as to correspond to half height of the fluorescence spectrum of a sensor, then the relationship between the ratio ( $R$ ) and conversion of reacting functional groups is linear.<sup>29</sup> Then the ratio change induced by the polymerization of each particular functional group ( $\Delta R_i$ ,  $i = 1$  or  $2$ ) can be expressed by eqn (5):

$$\Delta R_i = \Delta R_{i(100\%)} \cdot \alpha_i \quad (5)$$

where  $\Delta R_{i(100\%)}$  ( $i = 1$  or  $2$ ) is the ratio span that would be achieved in a pure monomer ( $i$ ) if all of the functional groups in the monomer polymerized with 100% conversion (which never happens in the case of multifunctional monomers), while  $\alpha_i$  is the actual functional group conversion. Hence, for a binary monomer system, it can be expected that the ratio change ( $\Delta R$ ) upon hybrid polymerization of a monomer mixture will be proportional to the actual conversions ( $\alpha_i$ ) of the particular functional groups ( $i$ ), and to volume fractions ( $\varphi_i$ ) of the particular monomers in the initial monomer mixture, according to eqn (6):

$$\Delta R = \Delta R_{1(100\%)} \alpha_1 \varphi_1 + \Delta R_{2(100\%)} \alpha_2 \varphi_2 \quad (6)$$

where  $\Delta R_{1(100\%)}$  and  $\Delta R_{2(100\%)}$  are the constants characteristic of each monomer/sensor system that are proportional to the sensor sensitivities.

It has to be pointed out that only in the case where the particular functional group conversions ( $\alpha_i$ ) in the monomer mixture are the same as the corresponding conversions achieved in pure monomers upon monomer polymerization under identical polymerization conditions, the relationship represented by eqn (6) is linear relative to the volume fraction of one of the components, as observed in the case of the TMPTA/CADE system. In fact, when it is noticed that the relationships between the variables in eqn (6) and those in eqn (3) are represented by eqn (7)–(11), substitution of eqn (7)–(11) to eqn (6) leads to theoretical derivation of eqn (3) that was found experimentally.

$$\Delta R = R_{\max} - 1 \quad (7)$$



$$\Delta R_{1(100\%)}\alpha_1 = R_{\max\_pureTMPTA} - 1 \quad (8)$$

$$\Delta R_{2(100\%)}\alpha_2 = R_{\max\_pureCADE} - 1 \quad (9)$$

$$\varphi_1 = \varphi_{TMPTA} \quad (10)$$

$$\varphi_2 = 1 - \varphi_{TMPTA} \quad (11)$$

On the other hand, the high nonlinearity observed in the case of the GlyMA/CADE system (Fig. 13) may be explained by the fact that when functional groups present in different monomers (*e.g.*, glycidyl groups in GlyMA and epoxycyclohexyl groups in CADE) copolymerize with each other, the kinetics of the copolymerization is different from the kinetics of particular homopolymerizations of pure monomers. Then the functional group conversions (*i.e.*,  $\alpha_1$  and  $\alpha_2$ ), achieved upon homopolymerization of pure monomers, are not the same as the corresponding conversions achieved in the monomer mixtures under identical polymerization conditions. Consequently, the overall polarity change caused by the polymerization of particular functional groups in the GlyMA/CADE monomer mixtures is different from that achieved in the case of pure monomers and  $\Delta R$  does not follow the linear relationship analogical to eqn (3). Moreover, in the case of the GlyMA/CADE system, the situation is further complicated, because in hybrid polymerization it behaves as a ternary system, where three different functional groups (*i.e.*, glycidyl, epoxycyclohexyl and methacrylic) participate in the hybrid photopolymerization, so a third component would have to be added to eqn (6).

## Conclusions

The *meta*-terphenyl derivatives reported in this paper can be applied as versatile fluorescent molecular sensors for monitoring the progress of free radical, cationic and hybrid polymerization processes by the FPT. The versatility of these sensors enables monitoring the progress of hybrid polymerization processes that was not possible with traditional fluorescent probes suitable only for one type of polymerization. All of the sensors (except for S-ST-2) exhibit high enough sensitivity and stability in polymerizing media to measure the polymerization progress precisely, using the fluorescence intensity ratio ( $R$ ) as the progress indicator.

Among the sensors studied, the S-Ph-5 sensor, containing a methylsulfanyl group in its structure, shows extremely high sensitivity to polarity changes occurring during cationic and free radical polymerization of monomers. In the case of cationic polymerization, the *m*-terphenyl derivatives containing electron-donating substituents at a conjugated position relative to one of the cyano groups present in their structure show higher sensitivity than those containing electron-withdrawing groups. The push–pull effect between electron-donating and electron-withdrawing substituents in the sensor structure, which increases the dipole moment of the sensor's excited state, also increases the sensor's sensitivity to polarity changes in its environment.

When diphenyliodonium hexafluorophosphate is used as a photoinitiator, glycidyl methacrylate (GlyMA) undergoes hybrid polymerization (*i.e.*, both cationic and free radical polymerization simultaneously). In the presence of a 2,2-dimethoxy-2-phenylacetophenone photoinitiator only free radical polymerization of the methacrylic groups of GlyMA occurs.

Hybrid photopolymerization of TMPTA/CADE mixtures induced by diphenyliodonium hexafluorophosphate leads to an ideal interpenetrating network, where the poly(TMPTA) network is formed by the free radical polymerization mechanism, while a poly(CADE) network is formed by cationic polymerization. During the hybrid polymerization of TMPTA/CADE mixtures, each monomer polymerizes independently and reaches the same final conversion as that achieved during the polymerization of the pure monomer. This leads to a linear relationship between the final fluorescence intensity ratio of a sensor and the volume fraction of one of the monomers in the mixture.

Hybrid photopolymerization of GlyMA/CADE mixtures leads to a crosslinked copolymer, where glycidyl groups of GlyMA are copolymerized with epoxycyclohexyl groups of CADE by cationic copolymerization, while methacrylic groups present in GlyMA form additional crosslinks by free radical polymerization. The overall final functional group conversions in the GlyMA/CADE copolymer are higher than the conversions achieved in the corresponding homopolymerization processes.

Photopolymerization profiles, obtained by the FPT using the sensors studied, show the difference between different types of polymerization processes involved in the hybrid polymerization of monomers. The implementation of the proposed fluorescent molecular sensors may be useful for the monitoring and control of complex processes such as the formation of interpenetrating polymer networks (IPNs) or copolymerizations involved in new applications, such as 3D printing.

## Author contributions

Conceptualization, J. Ortyl and R. Popielarz; software, R. Popielarz; investigation, M. Bilut and W. Tomal; data curation, W. Tomal, P. Szymaszek, and R. Popielarz; writing—original draft preparation, W. Tomal, R. Popielarz., P. Szymaszek and T. Świergorz; writing—review and editing, W. Tomal, R. Popielarz, and J. Ortyl; supervision, J. Ortyl; funding acquisition, J. Ortyl and W. Tomal.

## Conflicts of interest

There are no conflicts to declare.

## Acknowledgements

This research was funded by the Foundation for Polish Science (Warsaw Poland) – TEAM TECH project Grant No. TEAM



TECH/2016-2/15 (POIR.04.04.00-00-204B/16-00). The project: "WAY TO EXCELLENCE – a comprehensive university support program" implemented under the Operational Program Knowledge Education Development 2014-2020 co-financed by the European Social Fund WND-POWR.03.05.00-00-Z214/18 funded the publication of this manuscript in open access resources.

## Notes and references

- V. Perez-Puyana, M. Jiménez-Rosado, A. Romero and A. Guerrero, *Polymer*, 2020, **12**, 1566.
- E. Barrett-Catton, M. L. Ross and P. Asuri, *Polymer*, 2021, **13**, 856.
- K. Szczepanowicz, T. Kruk, W. Świątek, A. M. Bouzga, C. R. Simon and P. Warszyński, *Colloids Surf., B*, 2018, **166**, DOI: [10.1016/j.colsurfb.2018.03.020](https://doi.org/10.1016/j.colsurfb.2018.03.020).
- A. J. Nathanael and T. H. Oh, *Polymer*, 2020, **12**, 3061.
- M. Szczęch, N. Łopuszyńska, W. Tomal, K. Jasiński, W. P. Węglarz, P. Warszyński and K. Szczepanowicz, *Langmuir*, 2020, **36**, DOI: [10.1021/acs.langmuir.0c01512](https://doi.org/10.1021/acs.langmuir.0c01512).
- S. Mejlsoe and A. Kakkar, *Molecules*, 2020, **25**, 3995.
- Y. Yagci, S. Jockusch and N. J. Turro, *Macromolecules*, 2010, **43**, 6245–6260.
- S. Chatani, C. J. Kloxin and C. N. Bowman, *Polym. Chem.*, 2014, **5**, 2187–2201.
- P. Xiao, J. Zhang, F. Dumur, M. A. Tehfe, F. Morlet-Savary, B. Graff, D. Gignes, J. P. Fouassier and J. Lalevée, *Prog. Polym. Sci.*, 2015, **41**, 32–66.
- N. Corrigan, J. Yeow, P. Judzewitsch, J. Xu and C. Boyer, *Angew. Chem., Int. Ed.*, 2019, **58**, 5170–5189.
- I. Kamińska, J. Ortyl and R. Popielarz, *Polym. Test.*, 2016, **55**, 310–317.
- D. Nowak, J. Ortyl, I. Kamińska-Borek, K. Kukuła, M. Topa and R. Popielarz, *Polym. Test.*, 2017, **64**, 313–320.
- D. Nowak, J. Ortyl, I. Kamińska-Borek, K. Kukuła, M. Topa and R. Popielarz, *Polym. Test.*, 2018, **67**, 144–150.
- K. Kostrzewska, J. Ortyl, R. Dobosz and J. Kabatc, *Polym. Chem.*, 2017, **8**, 3464–3474.
- J. P. Fouassier, X. Allonas and D. Burget, *Prog. Org. Coat.*, 2003, **47**, 16–36.
- P. Glöckner and National Paint and Coatings Association, *Radiation curing: coatings and printing inks: technical basics, applications and trouble shooting*, Vincentz Network, 2008.
- W. Arthur Green, *Industrial Photoinitiators - A Technical Guide*, 2010.
- Z. Czech, A. Kowalczyk, J. Ortyl and J. Swiderska, *Pol. J. Chem. Technol.*, 2013, **15**, 12–14.
- B. Strehmel, S. Ernst, K. Reiner, D. Keil, H. Lindauer and H. Baumann, *Z. Phys. Chem.*, 2014, **228**, 129–153.
- C. Schmitz, Y. Pang, A. Gülz, M. Gläser, J. Horst, M. Jäger and B. Strehmel, *Angew. Chem., Int. Ed.*, 2019, **58**, 4400–4404.
- Z. Wang, W. Huang, P. Peng and D. E. Fennell, *Chemosphere*, 2010, **78**, 147–151.
- K. Nakamura, *Photopolymers: Photoresist Materials, Processes, and Applications*, CRC Press, 1st edn, 2014.
- H. Chen, G. Noirbent, K. Sun, D. Brunel, D. Gignes, F. Morlet-Savary, Y. Zhang, S. Liu, P. Xiao, F. Dumur and J. Lalevée, *Polym. Chem.*, 2020, **11**, 4647–4659.
- W. Tomal, D. Krok, A. Chachaj-Brekiesz, P. Lepcio and J. Ortyl, *Addit. Manuf.*, 2021, **48**, 102447.
- H. Mokbel, D. Anderson, R. Plenderleith, C. Dietlin, F. Morlet-Savary, F. Dumur, D. Gignes, J. P. Fouassier and J. Lalevée, *Prog. Org. Coat.*, 2019, **132**, 50–61.
- K. Lee, N. Corrigan and C. Boyer, *Angew. Chem., Int. Ed.*, 2021, **60**, 8839–8850.
- Z. Zhang, N. Athaniel Corrigan, A. Bagheri, J. Jin and C. Boyer, *Angew. Chem.*, 2019, **131**, 18122–18131.
- P. Fiedor, M. Pilch, P. Szymaszek, A. Chachaj-Brekiesz, M. Galek and J. Ortyl, *Catalysts*, 2020, **10**, 284.
- E. Hola, M. Topa, A. Chachaj-Brekiesz, M. Pilch, P. Fiedor, M. Galek and J. Ortyl, *RSC Adv.*, 2020, **10**, 7509–7522.
- E. Hola, M. Pilch, M. Galek and J. Ortyl, *Polym. Chem.*, 2020, **11**, 480–495.
- J. Ortyl, P. Fiedor, A. Chachaj-Brekiesz, M. Pilch, E. Hola and M. Galek, *Sensors*, 2019, **19**, 1668.
- K. Sawicz-Kryniger, P. Niezgodna, P. Stalmach, K. Starzak, A. Wysocka, T. Świergosz and R. Popielarz, *Eur. Polym. J.*, 2022, **162**, 110933.
- J. Ortyl, M. Galica, R. Popielarz and D. Bogdał, *Pol. J. Chem. Technol.*, 2014, **16**, 75–80.
- M. Topa, J. Ortyl, A. Chachaj-Brekiesz, I. Kamińska-Borek, M. Pilch and R. Popielarz, *Spectrochim. Acta, Part A*, 2018, **199**, 430–440.
- A. J. Lees, *Organometallic complexes as luminescence probes in monitoring thermal and photochemical polymerizations*, 1998, vol. 177.
- J. Ortyl, M. Topa, I. Kamińska-Borek and R. Popielarz, *Eur. Polym. J.*, 2019, **116**, 45–55.
- S. Hu, R. Popielarz and D. C. Neckers, *Fluorescence Probe Techniques (FPT) for Measuring the Relative Efficiencies of Free-Radical Photoinitiators*, 1998.
- M. E. Jolley, *Fluorescence Polarization: An Analytical Tool for Immunoassay and Drug Discovery*, 1999.
- J. C. Owicki, *J. Biomol. Screening*, 2000, **5**, 297–306.
- M. Z. Jonaghani, H. Zali-Boeini, R. Taheri, H. A. Rudbari and B. Askari, *RSC Adv.*, 2016, **6**, 34940–34945.
- K. Zhou, M. Ren, B. Deng and W. Lin, *New J. Chem.*, 2017, **41**, 11507–11511.
- J. Ortyl, K. Sawicz and R. Popielarz, *J. Polym. Sci., Part A: Polym. Chem.*, 2010, **48**, 4522–4528.
- M. A. Haidekker, T. P. Brady, D. Lichlyter and E. A. Theodorakis, *J. Am. Chem. Soc.*, 2006, **128**, 398–399.
- P. Bosch, F. Catalina, T. Corrales and C. Peinado, *Chem. – Eur. J.*, 2005, **11**, 4314–4325.
- I. Kamińska, J. Ortyl and R. Popielarz, *Polym. Test.*, 2015, **42**, 99–107.



- 46 W. P. Ambrose, P. M. Goodwin, J. H. Jett, A. van Orden, J. H. Werner and R. A. Keller, *Chem. Rev.*, 1999, **99**, 2929–2956.
- 47 J. R. Lakowicz, *Principles of fluorescence spectroscopy*, Springer, 2006.
- 48 D. L. Andrews, *Encyclopedia of applied spectroscopy*, Wiley-VCH, 2009.
- 49 W. Tomal, M. Pilch, A. Chachaj-Brekiesz, M. Galek, F. Morlet-Savary, B. Graff, C. Dietlin, J. Lalevée and J. Ortyl, *Polym. Chem.*, 2020, **11**, 4604–4621.
- 50 J. Ortyl and R. Popielarz, *J. Appl. Polym. Sci.*, 2013, **128**, 1974–1978.
- 51 J. Ortyl, J. Wilamowski, P. Milart, M. Galek and R. Popielarz, *Polym. Test.*, 2015, **48**, 151–159.
- 52 J. Ortyl, M. Galek, P. Milart and R. Popielarz, *Polym. Test.*, 2012, **31**, 466–473.
- 53 J. Ortyl, K. Sawicz and R. Popielarz, *J. Polym. Sci., Part A: Polym. Chem.*, 2010, **48**, 4522–4528.
- 54 M. J. M. Abadie and L. Jonescu-Vasii, Recent Advances in Cationic Photoinitiators – Application to the Photopolymerization of Epoxides and Vinyl Ethers, *Proceedings of RadTech Asia '95 Radiation Curing Conference*, Guilin, China, 1995, pp. 53–58.

